Ferroelectric phase transition in hydrogen-bonded 2-aminopyridine phosphate $(NC_4H_4NH_2)\cdot H_3PO_4$

2003 J. Phys.: Condens. Matter 15 3793

(http://iopscience.iop.org/0953-8984/15/22/313)

INSTITUTE OF PHYSICS PUBLISHING JOURNAL OF PHYSICS: CONDENSED MATTER

J. Phys.: Condens. Matter **15** (2003) 3793–3803 PII: S0953-8984(03)60540-0

Ferroelectric phase transition in hydrogen-bonded 2-aminopyridine phosphate $(NC_4H_4NH_2)\cdot H_3PO_4$

Z Czapla[1,3], **S Dacko**[1] **and A Waśkowska**[2]

[1] Institute of Experimental Physics, Wrocław University, M Borna 9, 50-204 Wrocław, Poland
[2] Institute of Low Temperature and Structure Research, Polish Academy of Sciences, Okólna 2, 50-422 Wrocław, Poland

E-mail: czapla@ifd.uni.wroc.pl

Received 7 March 2003
Published 23 May 2003
Online at stacks.iop.org/JPhysCM/15/3793

Abstract

A new crystal of 2-aminopyridine phosphate $(NC_4H_4NH_2)\cdot H_3PO_4$ has been grown and its x-ray structure and physical properties were studied. At room temperature the crystals are monoclinic, space group $C2/c$. The flat 2-aminopyridine cations are hydrogen bonded to the anionic $[PO_4]$ groups. The interesting feature of the crystal structure is the three-dimensional network of hydrogen bonds including, among others, two strong, symmetrical $O\cdots H, H\cdots O$ interactions with disordered proton locations. Symmetrically related PO_4 anions linked through these protons form infinite $(PO_4)_\infty$ chains along the crystal a-axis. The anomalies in the temperature dependence of the electric permittivity showed that the crystal undergoes ferroelectric phase transition at $T_c = 103.5$ K. The spontaneous polarization takes place along the crystal a-axis, being parallel to the chains of the hydrogen-bonded PO_4. The disordered protons, thermally activated at room temperature, can be frozen at their positions in the ferroelectric phase. The order–disorder continuous type of the transition has been evidenced on the basis of the temperature dependences of electric permittivity and spontaneous polarization measurements.

1. Introduction

Hydrogen-bonded compounds are interesting subjects of numerous studies in respect of fundamental properties of hydrogen bonds, dynamics of protons involved in these bonds and dipolar interaction leading to structural phase transitions in solid state. So far there are well known hydrogen-bonded phosphates and arsenates exhibiting ferroelectric or antiferroelectric properties. To this group belongs the widely described family of tetragonal KH_2PO_4

[3] Author to whom any correspondence should be addressed.

(e.g. [1, 2]), monoclinic CsH_2PO_4 [3], RbD_2PO_4 [4] and recently found monoclinic crystals containing organic cations like $(CH_3)_2NH_2H_2PO_4$ [5] and $(CH_3)_2NH_2H_2AsO_4$ [6]. Much attention has been devoted to the role of hydrogen bonding in the compounds exhibiting non-linear-optical properties and capable of generating second harmonics (e.g. [7, 8]). Systematic studies of these materials are directed toward finding a correlation between the structure and non-linear response with an aim of enhancing the non-linearities by structural modification [9, 10].

In the framework of our search for new hydrogen-bonded crystals, we synthesized the phosphate containing the 2-aminopyridine cation of formula $(NC_4H_4NH_2)\cdot H_3PO_4$, abbreviated as 2-APP. 2-aminopyridine is a compound with two different basic N atoms, i.e. one in the pyridinum ring and the second in the NH_2 group. Similarly as in other hydrogen-bonded phosphates the hydrogen atoms are expected to form intermolecular hydrogen bonds which influence the properties of this type of material. The purpose of the present study was to grow a single crystal of 2-APP and examine its symmetry and x-ray crystal structure in order to confirm the chemical formula and obtain information on intermolecular linkages in the structure. The essential aim of the work was to present the characteristics of basic properties of this material directed to the observation of potentially possible phase transitions.

2. Experimental details

2.1. Crystal growth

The polycrystalline form of 2-APP was obtained from a solution containing 2-aminopyridine and phosphorous acid in molar ratio 1:1. The polycrystalline reaction product was re-crystallized and next dissolved in water. Single crystals were grown from a saturated solution by the slow evaporation method at constant temperature of 304 K. Large crystals of good quality and volume of about 4 cm^3 were easily grown in a period of 4–5 weeks. Their shape was characteristic of the monoclinic system. The crystals were usually elongated in the [101] direction.

2.2. X-ray diffraction

A crystal of dimensions 0.28 mm $\times$ 0.22 mm $\times$ 0.20 mm was chosen for the x-ray diffraction measurements on a four-circle KM-4/CCD diffractometer (Oxford Diffraction). The intensity data were collected using graphite monochromated Mo Kα radiation ($\lambda = 0.71073$ Å) and the ω-scan technique with $\Delta\omega = 0.8°$. The 1200 images taken in seven different runs covered about 92% of the Ewald sphere. The exposure time for each frame was 20 s. To control stability of the crystal and electronic systems, one image selected as a standard was monitored after every 50 images. The unit cell parameters were determined and refined by a least-squares fitting of angular positions of 1100 strongest reflections. The reflection intensities were integrated and corrected for Lorentz and polarization effects [11]. Absorption correction was not applied, as the absorption coefficient was $\mu = 0.316$ mm^{-1}.

The structure was solved by direct methods using the SHELXS program [12] and refined with anisotropic thermal displacement parameters for non-hydrogen atoms [13]. H atoms were located in the difference maps. Their positional and isotropic thermal parameters were allowed to vary without constraints at the final stages of calculations. Two of the H atoms showed positional disorder and were not included in the refinement. A summary of the crystal data, details of experimental conditions and the structure refinement parameters are given in table 1.

Table 1. Crystal data, experimental conditions and the structure refinement parameters.

Empirical formula	$C_5H_9N_2O_4P$
Formula weight	192.10
Temperature (K)	293(2)
Wavelength (Å)	0.710 73
Crystal system, space group	Monoclinic, $C2/c$
Unit cell dimensions (Å)	$a = 13.484(3)$
	$b = 10.223(2)$
	$c = 12.602(3)$
	$\beta = 110.95(3)^\circ$
Volume ($Å^{-3}$)	1622.3(6)
Z, Calculated density (Mg m^{-3})	8, 1.557
Absorption coefficient (mm^{-1})	0.316 mm^{-1}
$F(000)$	784
Crystal size (mm)	$0.28 \times 0.23 \times 20$
θ range for data collection (deg)	3.40–47.31
Limiting indices	$-18 \leqslant h \leqslant 27, -20 \leqslant k \leqslant 16, -23 \leqslant l \leqslant 25$
Reflections collected/unique	17 159/6327[$R(int) = 0.0176$]
Refinement method	Full-matrix least squares on F^2
Data/restraints/parameters	6327/0/142
Goodness of fit on F^2	0.913
Final R indices [$I > \sigma(I)$]	$R_1 = 0.0441, wR_2 = 0.0851$
R indices (all data)	$R_1 = 0.0755, wR_2 = 0.0950$
Extinction coefficient	0.0163(4)
Largest diff. peak and hole (e $Å^{-3}$)	0.588 and −0.414

2.3. Dielectric and spontaneous polarization measurements

Dielectric permittivity was measured along three perpendicular crystallographic directions a, b and c^*, where $c^* = (c \sin \beta)^{-1}$ is perpendicular both to the a- and b-axes. The measurements were made using an HP 4010 A LCR meter at the frequency of 1 kHz and measuring field amplitude 100 V m^{-1}. Hysteresis loops were observed using a Diamant–Drenck–Pepinsky circuit.

Pyroelectric properties were examined using a UNITRA type 219 A electrometer on a heating run at constant $dT/dt = 1$ K min^{-1} and constant electric field of 2 kV m^{-1} applied in order to keep the sample in the monodomain state. All these studies were carried out in the temperature range 300–80 K.

3. Results and discussion

3.1. Crystal structure

The final atomic coordinates and equivalent isotropic displacement parameters U_{eq} are listed in table 2. The molecular structure consists of protonated 2-aminopyridine cations $(2\text{-apyH})^+$ hydrogen bonded to PO_4 anions (figure 1). The flat pyridine ring shows the characteristic sequence of short–long–short bond distances (table 3). The C–C and C–N bond lengths range from 1.350(2) to 1.412(2) Å and 1.330(2) to 1.361(2) Å, respectively. The molecular geometry is similar to that observed in related pyridine containing compounds [14, 15]. The N atom of the amino group with its hydrogen atoms lies in the plane of the ring. Both H atoms of the amino group are involved in hydrogen bonds. The PO_4 tetrahedron shows a distortion characteristic of the involvement of the O atoms in the intermolecular contacts. The mean

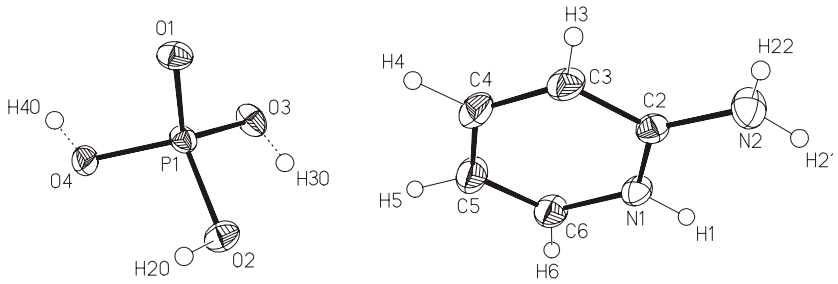

Figure 1. Molecular structure with atom labelling scheme. The ellipsoids of the thermal displacements are at 30% probability level.

Table 2. Atomic coordinates ($\times 10^4$) and equivalent isotropic displacement parameters (Å$^2 \times 10^3$). $U_{(eq)}$ is defined as one-third of the trace of the orthogonalized U_{ij} tensor.

	x	y	z	$U_{(eq)}$
P(1)	4063(1)	1297(1)	867(1)	26(1)
O(1)	3645(1)	1079(1)	1812(1)	31(1)
O(2)	5131(1)	2093(1)	1296(1)	35(1)
O(3)	3318(1)	2103(1)	−122(1)	35(1)
O(4)	4294(1)	−24(1)	412(1)	36(1)
N(1)	3796(1)	7584(1)	1081(1)	33(1)
N(2)	3440(1)	8455(1)	2598(1)	45(1)
C(2)	3550(1)	7412(1)	2020(1)	31(1)
C(3)	3428(1)	6116(1)	2337(1)	40(1)
C(4)	3565(1)	5099(1)	1709(1)	47(1)
C(5)	3812(1)	5320(1)	731(1)	48(1)
C(6)	3919(1)	6567(1)	440(1)	42(1)

P–O distance is 1.538(1) Å and the tetrahedral angles vary from 104.77(5)° to 113.60(5)° (table 3). All O atoms participate in intermolecular hydrogen bonding.

In the crystal structure the PO_4 groups linked through the hydrogen atoms form chains running in the [100] direction (figure 2). Within the three-dimensional network of hydrogen bonds stabilizing the present structure, there can be distinguished two main types of those linkages. The first type includes connections joining two PO_4 anions, related by a centre of symmetry, where the proton position is disordered about the centre. These so-called 'symmetrical' hydrogen bonds were found between $O(3)\cdots H, H\cdots O(3)_{1/2-x,1/2-y,-z}$ and $O(4)\cdots H, H\cdots O(4)_{1-x,-y,-z}$ with the short donor–acceptor distances of 2.471(2) and 2.469(2) Å, respectively and the average proton position H(30) at the 4(c), (1/4, 1/4, 0), site and H(4) at 4(a), (0, 1/2, 0), respectively. In the second group of HB, the protons were ordered at their positions as observed in $O(1)\text{–}H20\cdots O(2)_{1-x,y,-z}$ bridging another pair of the anions. Of the same type are the $N\text{–}H\cdots O$ and $C\text{–}H\cdots O$ bonds connecting the flat 2-apyH$^+$ units with the anionic groups. In this way the 2-aminopyridine acts as the structure-stabilizing unit. The geometrical details of the proposed hydrogen bonds are given in table 4.

3.2. Dielectric properties

The initial studies showed large anomalies of permittivity (ε) at 103.5 K in the ($a \times c$) plane. Taking into account the structural properties we expected to observe the maximum value of

Table 3. Bond lengths (Å) and angles (degrees).

P(1)–O(1)	1.5058(8)
P(1)–O(3)	1.5321(9)
P(1)–O(4)	1.5409(8)
P(1)–O(2)	1.5718(9)
O(2)–H(20)	0.964(18)
N(1)–C(2)	1.3496(13)
N(1)–C(6)	1.3630(16)
N(1)–H(1)	0.888(16)
N(2)–C(2)	1.3291(15)
N(2)–H(2A)	0.902(17)
N(2)–H(2B)	0.801(17)
C(2)–C(3)	1.4106(16)
C(3)–C(4)	1.3585(19)
C(3)–H(3)	0.916(16)
C(4)–C(5)	1.4053(19)
C(4)–H(4)	1.009(18)
C(5)–C(6)	1.3486(18)
C(5)–H(5)	0.956(18)
C(6)–H(6)	0.939(16)
O(1)–P(1)–O(3)	113.60(5)
O(1)–P(1)–O(4)	110.33(5)
O(3)–P(1)–O(4)	109.27(5)
O(1)–P(1)–O(2)	111.13(5)
O(3)–P(1)–O(2)	104.77(5)
O(4)–P(1)–O(2)	107.44(5)
P(1)–O(2)–H(20)	110.7(11)
C(2)–N(1)–C(6)	122.71(10)
C(2)–N(1)–H(1)	118.5(10)
C(6)–N(1)–H(1)	118.8(10)
C(2)–N(2)–H(2A)	120.1(10)
C(2)–N(2)–H(2B)	117.5(12)
H(2A)–N(2)–H(2B)	122.1(16)
N(2)–C(2)–N(1)	119.12(10)
N(2)–C(2)–C(3)	123.41(10)
N(1)–C(2)–C(3)	117.47(10)
C(4)–C(3)–C(2)	119.96(11)
C(4)–C(3)–H(3)	121.9(11)
C(2)–C(3)–H(3)	118.1(11)
C(3)–C(4)–C(5)	120.84(11)
C(3)–C(4)–H(4)	118.5(10)
C(5)–C(4)–H(4)	120.6(10)
C(6)–C(5)–C(4)	118.19(12)
C(6)–C(5)–H(5)	121.2(11)
C(4)–C(5)–H(5)	120.6(11)
C(5)–C(6)–N(1)	120.83(11)
C(5)–C(6)–H(6)	123.5(10)
N(1)–C(6)–H(6)	115.6(10)

permittivity along the direction of the hydrogen-bonded chains of PO_4. The temperature dependence of the electric permittivity along the a-axis is shown in figure 3. The permittivity increases considerably starting below 108 K and it reaches a maximum equal to 70 000 at $T_c = 103.5$ K. Below this temperature the permittivity decreases. This type of anomaly is

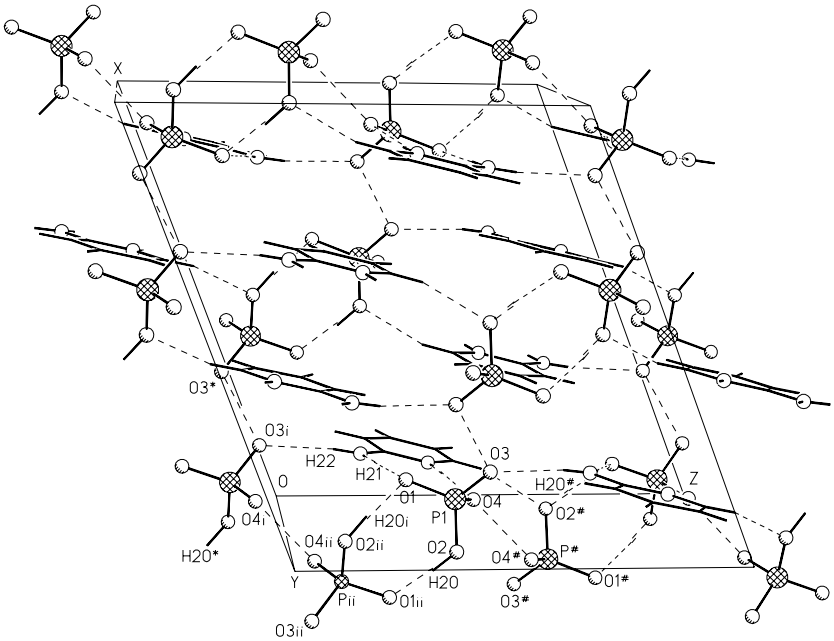

Figure 2. Crystal structure of 2-APP with the proposed hydrogen bonding system.

Table 4. Short intermolecular distances and proposed hydrogen bonds: symmetry transformations used to generate equivalent atoms. #1, $1/2-x$, $1/2-y$, $-z$; #2, $1-x$, $-y$, $-z$; #3, $1-x$, y, $1/2-z$; #4, x, $y+1$, z; #5, x, $-y+1$, $z+1/2$; #6, $1-x$, $1-y$, $-z$.

D–H···A	d(D–H)	d(H···A)	d(D···A)	<(DHA)
O(3)–H(30)···O(3)#1			2.4686(16)	
O(4)–H(40)···O(4)#2			2.4740(15)	
O(2)–H(20)···O(1)#3	0.964(18)	1.622(18)	2.5823(14)	173.8(17)
N(1)–H(1)O(4)#4	0.892(16)	1.868(17)	2.7469(13)	168.1(16)
N(2)–H(2A)···O(1)#4	0.902(17)	2.006(17)	2.9071(15)	177.9(15)
N(2)–H(2B)···O(3)#5	0.801(17)	2.195(18)	2.9913(15)	172.6(17)
C(6)–H(6)···O(2)#6	0.939(16)	2.314(16)	3.2104(15)	159.5(13)

characteristic of the ferroelectric phase transition and therefore, the low-temperature phase is expected to exhibit ferroelectric properties. The temperature dependence of the permittivity obeys the Curie–Weiss law in the paraelectric phase starting from room temperature down to T_c. The Curie–Weiss constant $C_p = 12.2 \times 10^3$ K, $T_0 = T_c$ and $\varepsilon_\infty = 9.5$ pointing to the continuous character of the transition. The value of the Curie–Weiss constant appeared to be four times larger than in the known triglycine sulfate (TGS) [16] and comparable with the Curie–Weiss constant observed in hydrogen-bonded betaine phosphite (BPI) with the order–disorder type of phase transition [17] but about 15 times smaller in comparison to barium titanate [18]. This comparison suggests the order–disorder type of phase transition. The Curie–Weiss law is fulfilled in the ferroelectric phase in the range of about 10 K below T_c. The value of the Curie–Weiss constant C_f is equal to 2.90×10^3 K. The ratio of C_p/C_f is equal to about 4.2 and this means that the phase transition is continuous but close to a critical one.

The temperature dependences of the permittivity along the b- and c^*-axes are shown in figure 4. The permittivity measured along the c^*-axis has an anomaly at 103.5 K. The maximum

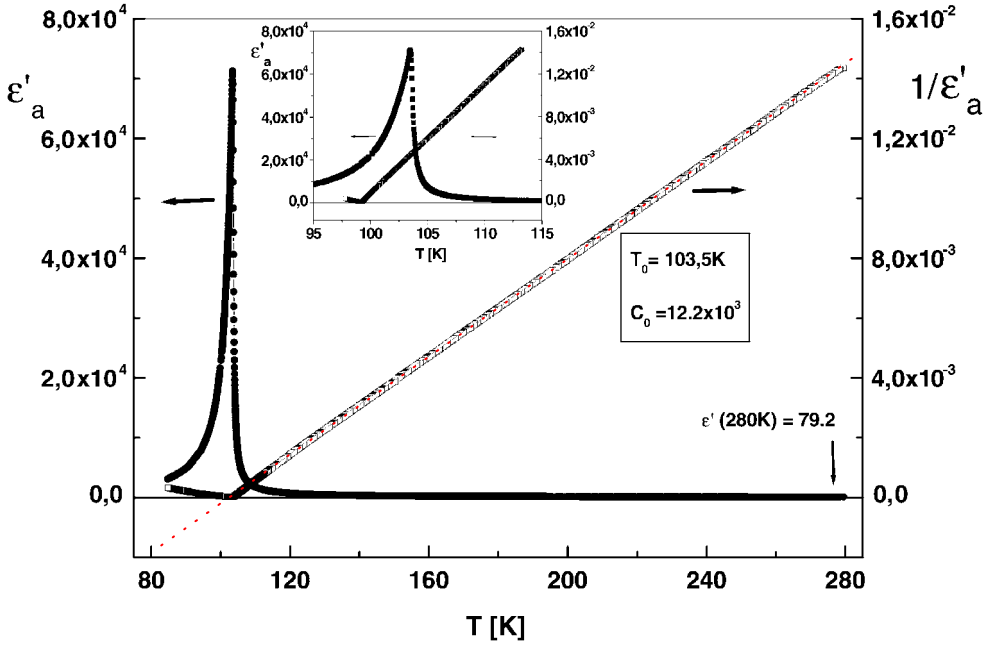

Figure 3. Temperature dependence of electric permittivity measured along the *a*-axis and the Curie–Weiss law fulfilment in 2-APP.

(This figure is in colour only in the electronic version)

value of the permittivity at the phase transition is equal to about 700, being much smaller than the value measured along the [100] direction. Thus, it can be assumed that the ferroelectric axis runs along the [100] direction or at least very close to it. Along the monoclinic *b*-axis the permittivity increase is clearly seen on the cooling run. An anomalous value of permittivity equal to 35 is observed at T_c and below this temperature the permittivity decreases.

3.3. Spontaneous polarization

Hysteresis loops are easily observed below the transition temperature and for some chosen temperatures they are presented in figure 5. These observations proved 2-APP to be a ferroelectric below below 103.5 K. Since the value of spontaneous polarization (P_s) was not very large and coercive field (E_c) was rather low, it appeared difficult to measure P_s with high accuracy, especially very close to the phase transition temperature. Therefore, to determine the temperature dependent variation of P_s more precisely, we have studied the pyroelectric properties of the crystal. To keep the sample in a monodomain state the electric field of 2 kV m^{-1} was applied when measuring the pyroelectric coefficient. A contribution of the applied electric field to the electric current is insignificant, as could be concluded from the measurement in the para-phase, where no current was observed.

The temperature dependences of the pyroelectric coefficient and spontaneous polarization P_s (integer of γ) related at constant heating rate by $\gamma = \mathrm{d}P_s/\mathrm{d}T$ are shown in figure 6. To find a real dependence of γ and P_s the charge induced by electric field was subtracted from the charge measured in experiment. An appearance of spontaneous polarization is characteristic of a continuous phase transition. At temperatures far from T_c the value of spontaneous polarization

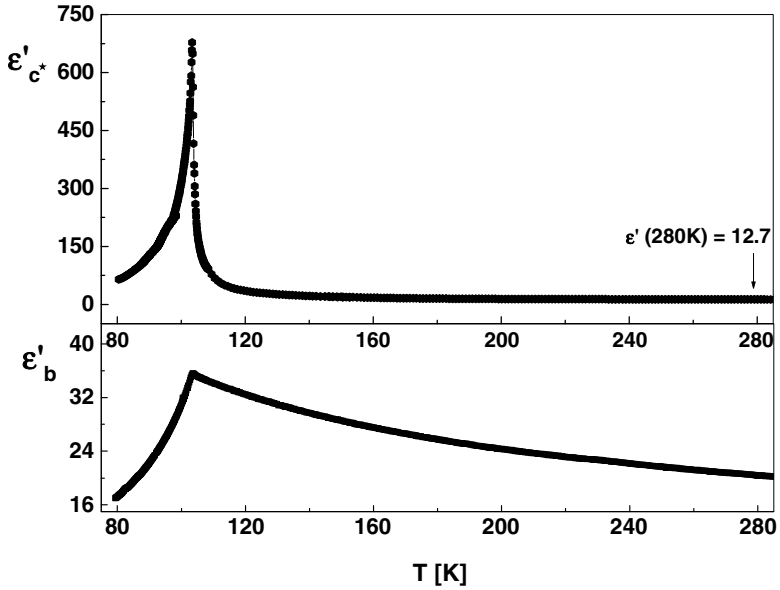

Figure 4. The temperature dependences of electric permittivity in 2-APP (along the *b*- and c^*-axes, where $c^* = (c \sin \beta)^{-1}$).

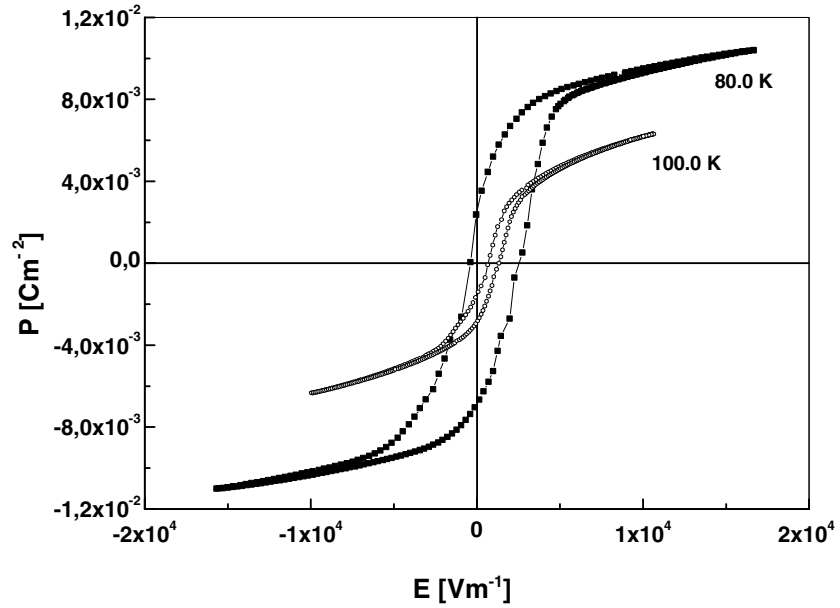

Figure 5. The hysteresis loops observed in the 2-APP crystal.

obtained from pyroelectric studies corresponds well to that observed from the hysteresis loops. The reversal of polarization is also confirmed.

To verify in more detail the thermodynamic nature of the transition we have referred to the classical Landau theory as described in (e.g. [19, 20]). The temperature dependent behaviour

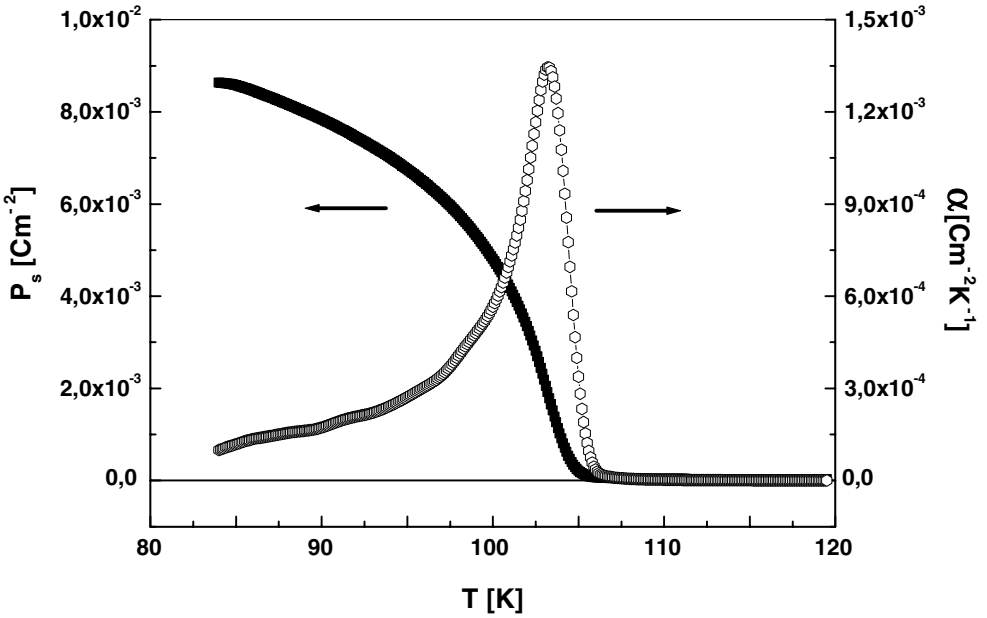

Figure 6. The temperature dependences of pyroelectric coefficient and the spontaneous polarization in 2-APP measured along the a-axis.

of P_s shows that it may be considered as an order parameter. Following the theory the order parameter η is expected to vary with temperature as

$$\eta \sim P_s \sim |T_c - T|^{2\beta}$$

where β, the critical exponent, takes the value $0.25 < \beta \leqslant 0.5$ for continuous phase transitions. In figure 7 characteristics of P_s^2 and P_s^4 are shown as a function of temperature in a wide temperature range. As can be seen in figure 7 the linear dependence of P_s^2 is valid only in the vicinity of T_c and in the case of P_s^4 linearity is preserved in a broad temperature range excluding the vicinity of the phase transition temperature. On the grounds of these experimental results it can be concluded that the phase transition is continuous and close to a critical one [19, 20].

3.4. Molecular mechanism of the phase transition

On the basis of the results and arguments given above it can be stated that 2-APP is a new ferroelectric material with the spontaneous polarization as an order parameter. At room temperature both the 2-aminopyridine and the PO_4 tetrahedron form rigid groups with atom locations well defined, which do not show any features suggesting vibrational or positional disorder. In the context of the structure description it can be assumed that the driving force for the transition is the order–disorder behaviour of the protons in hydrogen bonds. The essential role can be ascribed to the protons of two symmetrical hydrogen bonds, which, thermally activated at room temperature, will be frozen in ordered positions below T_c, giving rise to the appearance of non-compensated dipole moments, revealed as the macroscopic spontaneous polarization in the ferroelectric phase. The symmetry of the ferroelectric phase is expected to be monoclinic with space group Cc.

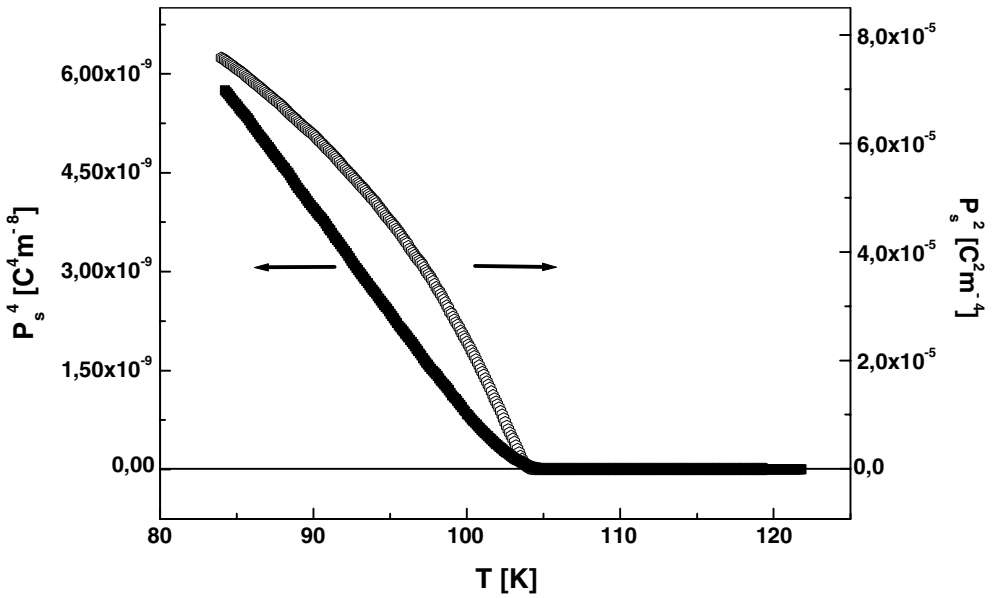

Figure 7. The temperature dependences of P_s^2 and P_s^4 in 2-APP.

4. Summary

(1) The new compound, 2-aminopyridine dihydrogen phosphate, at room temperature belongs to the monoclinic system, space group $C2/c$. The x-ray diffraction studies revealed short hydrogen bonds with disordered protons, linking the PO_4 tetrahedra in the chains directed along the crystallographic a-axis.
(2) The 2-APP crystal exhibits ferroelectric properties below $T_c = 103.5$ K. The Curie–Weiss law is fulfilled well in a very broad temperature range with the Curie–Weiss constant $C_p = 12.2 \times 10^3$ K.
(3) Spontaneous polarization is directed along the crystallographic a-axis and at 80 K reaches the value of 8.7×10^{-3} C m^{-2}.
(4) The molecular mechanism of the ferroelectric phase transition is most probably related to the proton ordering in the short hydrogen bonds of the type O $\cdots$ H, H $\cdots$ O.

Acknowledgment

The work was supported by the University of Wrocław under Grant 2016/W/IFD/03.

References

[1] Nelmes R J 1984 *Ferroelectrics* **53** 207
[2] Nelmes R J 1982 *J. Phys. C: Solid State Phys.* **15** 59
[3] Matsunaga K, Itoh K and Nakamura E 1980 *J. Phys. Soc. Japan* **49** 2011
[4] Sumita M, Osaka T and Makita Y 1981 *J. Phys. Soc. Japan* **50** 154
[5] Hatori J, Komukae M, Osaka T and Makita Y 1996 *J. Phys. Soc. Japan* **65** 1960
[6] Hatori J, Komukae M and Osaka T 1997 *J. Phys. Soc. Japan* **66** 4031
[7] Xue D F and Zhang S Y 1996 *J. Phys. Chem. Solids* **57** 1321
[8] Xue D F and Zhang S Y 1999 *Chem. Phys. Lett.* **301** 449

[9] Debrus S *et al* 2002 *Synth. Met.* **127** 99 (special issue)
[10] Xue D and Ratajczak H 2003 *Chem. Phys. Lett.* **371** 601
[11] Oxford Diffraction 2001 *CrysAlis 'CCD' and CrysAlis 'RED'* (Wrocław: Oxford Diffraction)
[12] Sheldrick G M 1997 *SHELXS97, Program for Solution of Crystal Structures* University of Göttingen
[13] Sheldrick G M 1997 *SHELXL97, Program for Crystal Structure Refinement* University of Göttingen
[14] Low J N, Ferguson G, Cobo J, Melguizo M, Nogueras M and Sanchez A 1996 *Acta Crystallogr.* C **52**
[15] Hanuza J, Michalski J, Mączka M, Waśkowska A, Talik Z and van der Maas J H 2002 *J. Raman Spectrosc.* **33** 229
[16] Matthias B T, Miller C E and Remeika J P 1956 *Phys. Rev.* **104** 849
[17] Sobiestianskas R, Grigas J, Czapla Z and Dacko S 1993 *Phys. Status Solidi* a **136** 223
[18] Drougard M E and Young D R 1954 *Phys. Rev.* **95** 1152
[19] Blinc R and Zeks B 1974 *Soft Modes in Ferroelectrics and Antiferroelectrics* (Amsterdam: North-Holland)
[20] Strukov B A and Levanyuk A P 1995 *Fizicheskiye Osnovi Segnetoelektricheskyh Yavleniy v kristallah* (Moscow: Nauka)